Optical Materials 66 (2017) 519–526

Contents lists available at ScienceDirect

Optical Materials

journal homepage: www.elsevier.com/locate/optmat

Excited state absorption and energy transfer in Ho^{3+}-doped indium fluoride glass

Laercio Gomes [a], Vincent Fortin [b], Martin Bernier [b], Frédéric Maes [b], Réal Vallée [b], Samuel Poulain [c], Marcel Poulain [c], Stuart D. Jackson [d, *]

[a] Center for Lasers and Applications, IPEN/CNEN-SP, P.O. Box 11049, São Paulo, SP, 05422-970, Brazil
[b] Center for Optics, Photonics and Lasers (COPL), Université Laval, Québec, G1V 0A6, Canada
[c] Le Verre Fluoré, Campus KerLann, F-35170, Bruz, Brittany, France
[d] MQ Photonics, Department of Engineering, Faculty of Science and Engineering, Macquarie University, North Ryde, 2109 Australia

ARTICLE INFO

Article history:
Received 16 January 2017
Received in revised form
20 February 2017
Accepted 23 February 2017
Available online 9 March 2017

ABSTRACT

This investigation examines in detail the rates of energy transfer relevant to the $^5I_5 \rightarrow {}^5I_6$ transition (at 3930 nm) in Ho^{3+}-doped InF_3 glass as a function of the Ho^{3+} concentration. The decay times, branching ratios and rate parameters for energy transfer were measured in this investigation for Ho^{3+} (x)-doped InF_3 glass with x = 2, 4 and 10 mol.% and they were used as the input parameters for a rate equation analysis. Excited state absorption (ESA) initiating from the lower laser level is included in the study. Numerical simulation of CW laser emission at 3.9 μm was performed using two pump wavelengths, one for upper laser level excitation (i.e., $^5I_8 \rightarrow {}^5I_5 = \lambda_{P1}$) and the other for lower laser level de-excitation (i.e., $^5I_6 \rightarrow {}^5S_2 = \lambda_{P2}$). The pump wavelength $\lambda_{P2} = 962$ nm was chosen based on the measurements of ESA and the application of the McCumber method. Critically, the estimated ESA cross section at $\lambda_{P2} = 962$ nm ($\sigma_{ESA} = 7.1 \times 10^{-21}$ cm^2) is approximately sixteen times larger than ground state ($^5I_8$) absorption cross section ($\sigma_{GSA} = 4.3 \times 10^{-22}$ cm^2) and ESA does not overlap with any ground state absorption process. Our calculations suggest that even for high Ho^{3+} concentration in which cross relaxation has been shown in a previous study to quench the $^5I_5$ level, ESA is nevertheless strong enough to allow a sufficient population inversion required for practical CW emission.

1. Introduction

The quest longer wavelength emission from a fibre laser is largely driven by applications accessing atmospheric transmission windows and the convenient overlap with strong molecular absorption. Since the first demonstration of 3.9 μm emission from Ho^{3+}-doped ZBLAN glass fibre quite some time ago [1,2] very little progress has been demonstrated in either increasing the output power or efficiency from rare earth doped fibres emitting in this region. This situation has resulted from two competing issues. First, the $^5I_5 \rightarrow {}^5I_6$ transition (at 3930 nm) of Ho^{3+} has not been easy to access because until recently, high power pump sources that directly excite the upper laser level at approximately 890 nm were not widely available. The other problem relates to the traditional use of ZBLAN glass because multiphonon absorption in this glass limits the both the luminescence efficiency of the $^5I_5 \rightarrow {}^5I_6$ transition and the transmission efficiency of 3.9 μm photons. This latter feature is a particular issue for a fibre geometry.

The recent demonstration [3] of mJ-level output from this transition using bulk Ho^{3+}-doped indium fluoride glass has initiated a revival of research into this transition. Not only did this demonstration show that a fluoride-glass based host is a suitable material for efficient near 4 μm laser emission but it also represented the first use of Ho^{3+}-doped InF_3 glass for laser applications. Indium fluoride glasses have a comparatively lower phonon energy allowing better infrared transmission and this glass has been shown to be an excellent source of low loss fibre [4]. Research can now be directed towards the development and optimisation of Ho^{3+}-doped InF_3 glass for fibre laser emission in the 4 μm region and beyond.

Recently [5], we elucidated the primary spectroscopic parameters of Ho^{3+}-doped InF_3 glass in terms of the absorption and emission cross sections and energy transfer parameters for a single

* Corresponding author.
E-mail address: stuart.jackson@mq.edu.au (S.D. Jackson).

http://dx.doi.org/10.1016/j.optmat.2017.02.048
0925-3467/

Ho^{3+} concentration of 10 mol.%. In this earlier study, a cross relaxation process was identified as having a strong quenching effect on the decay time of the $^5I_5$ upper laser level. In the current study, we cover a wide concentration range in order extract the rate parameters for energy transfer of all the known energy transfer pathways relevant to the $^5I_5 \rightarrow {}^5I_6$ transition. In addition, we examine excited state absorption at a wavelength of 962 nm that initiates from the lower ($^5I_6$) level and show, by way of numerical simulation, that it has a beneficial effect on laser performance and allows access to much higher Ho^{3+} concentrations than thought possible given the known detrimental effects from cross relaxation at high Ho^{3+} concentration.

2. Experimental procedure

The composition of the glass samples used has been discussed in detail in our previous investigation [5]. All samples were prepared from 99.99% pure fluoroindate salts GaF_3, BaF_2, SrF_2, ZnF_2 and HoF_3 based on the pioneering work found in the literature [6–9]. The samples were melted in a dry box to reduce the water content, the melt was poured into brass moulds and the samples cut and polished into rectangular prisms. The Ho^{3+} ion densities in the 2 mol.%, 4 mol.% and 10 mol.% samples were calculated to be 4×10^{20} cm^{-3}, 8×10^{20} cm^{-3} and 2×10^{21} cm^{-3}, respectively.

We used an optical parametric oscillator as a tunable pulsed pump source that could provide direct excitation to all the energy levels of interest. The pulse energies incident on the samples were up to 15 mJ, the pulse durations were 4 ns, and the repetition frequency was 10 Hz. A Judson model J-10 D InSb infrared detector (cooled to 77 K) was used to detect the infrared luminescence (for wavelengths longer than 1080 nm). A fast preamplifier (response time ~0.5 μs) was used to amplify the signal. A photomultiplier tube (EMI, response time 10 ns) was employed to detect the visible and near infrared (i.e., λ < 1100 nm) luminescence. All measurements were carried out at 300 K. Bandpass filters each with ~80% transmission at 1200 nm, 2100 nm and 4000 nm with a half width of 25 nm and an extinction coefficient of approximately 10^{-5} outside this band were used to isolate the relevant infrared luminescence.

3. Experimental results

The following equations and fitting parameters that were used to fit the measured fluorescence decay and upconversion luminescence transients of Ho^{3+}-doped InF_3 glass have been discussed in detail in our previous investigation [5] and interested readers can refer to this study.

3.1. Luminescence decay and cross relaxation from the $^5I_5$ level

Fig. 1 shows the simplified energy level diagram of the Ho^{3+} ion used for the analysis of the experimental results and the rate equation model presented later. Fig. 2 shows measured fluorescence decay from the $^5I_5$ level for the Ho^{3+}-doped InF_3 glasses after pulsed laser excitation at 889 nm. The experimental luminescence decays were fitted using [5].

$$I(t) = I_0 \exp\left(-\gamma\sqrt{t} - t/t_1\right), \tag{1}$$

where γ ($s^{-1/2}$) is the energy transfer (CR) parameter and t_1 is the time constant of the exponential part of the decay. The integrated lifetime was obtained using

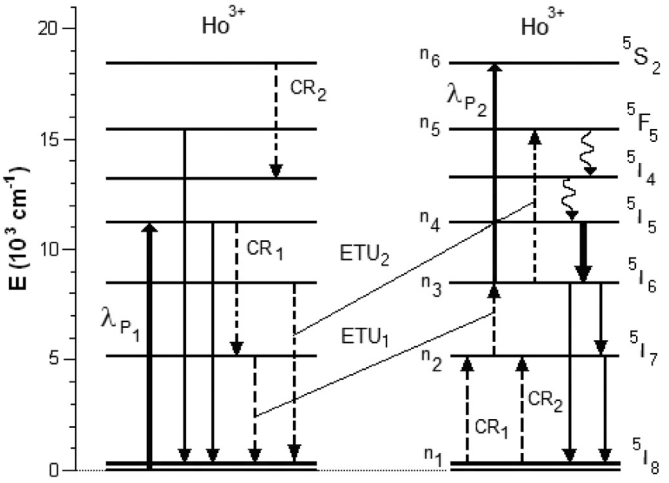

Fig. 1. Schematic energy level diagram used to show all the processes involved in the numerical model describing laser emission at 3.93 μm (due to the $^5I_5 \rightarrow {}^5I_6$ transition) after laser pumping at 889 nm (λ_{P1}) and the secondary laser pumping at 962 nm (λ_{P2}). CR_1 and CR_2 are used to represent the cross-relaxations processes.

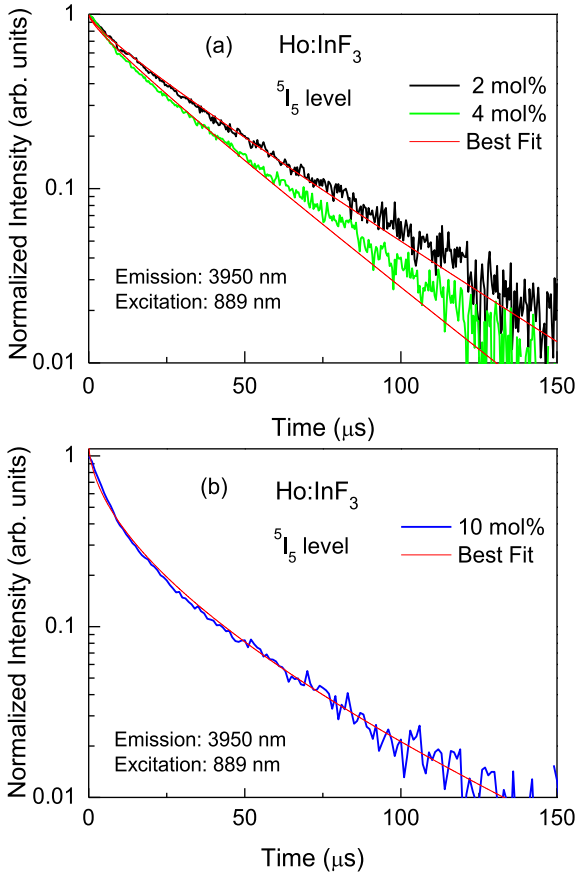

Fig. 2. Measured luminescence decay from the $^5I_5$ level after pulsed laser excitation at 889 nm (with a mean pulse energy of 6 mJ) for the Ho(x):InF_3 glasses with (a) x = 2, 4 and (b) 10 mol.% - data taken from Ref. [5].

$$\tau = \frac{1}{I_0}\int_0^\infty I(t)\,dt. \tag{2}$$

The best-fit parameters using these equations are giving in Table 1.

Table 1
The cross-relaxation rate and cross-relaxation efficiencies relevant to the luminescence decay of the $^5I_5$ level.

[Ho] (mol.%)	γ ($s^{-1/2}$)	t_1 (μs)	R^2	τ_1(int) (μs) (integrated)	W_{CR1} (s^{-1})	η_{CR1}
2	66	42.4	0.996	30	25926	0.795
4	62	33.5	0.994	24	34259	0.837
10	333	135	0.992	13	69516	0.913

As observed from Fig. 2, it is clear that a nonradiative quenching process is acting on the $^5I_5$ level with increased Ho^{3+} ion concentration. We have previously identified [5] that a cross-relaxation process (labelled CR_1) competes with the intrinsic decay of the $^5I_5$ level and that the cross relaxation process is a resonant interaction between two Ho^{3+} ions according to the process: Ho^{3+} ($^5I_5$) + Ho^{3+} ($^5I_8$) → Ho^{3+} ($^5I_7$) + Ho^{3+} ($^5I_7$). This non-radiative dipole-dipole interaction decreases the total lifetime of the $^5I_5$ level and its respective rate (in s^{-1}). The rate of CR_1 can be obtained using the relation: $W_{CR_1} = \frac{1}{\tau_1(\text{int})} - \frac{1}{\tau_d}$, where τ_d = 135 μs, which was determined in our previous report [5]. The cross-relaxation efficiency, defined as $\eta_{CR_1} = 1 - \frac{\tau_1(\text{int})}{\tau_d}$, can be used to determine the degree of nonradiative quenching resulting from this process. The parameters relevant to CR_1 are given in Table 1.

Fig. 2 shows the efficiency of the cross-relaxation process (i.e., η_{CR1}) as a function of the Ho^{3+} ion concentration. The solid red line shows the curve of best fit using the critical radius model, which assumes the existence of a critical radius R_C for the CR_1 process [5]. The use of the critical radius model is reliant on the following conditions: i) $\eta_{CR1} = \eta_0$ (constant) for all excited Ho^{3+}ions (in the $^5I_5$ level) having a nearby Ho^{3+}ground state ion within a distance $R \leq R_C$, and ii) $\eta_{CR1} = 0$ when $R > R_C$. If we consider a statistical distribution of Ho^{3+} ions in the glass matrix, we can obtain the cross-relaxation efficiency as a function of the Ho^{3+} concentration using

$$\eta_{CR1} = \eta_0 \{ 1 - \exp(-N/N_C) \}, \quad (3)$$

where $N_C = \left[\frac{4}{3}\pi R_C^3\right]^{-1}$, and η_0 is the constant efficiency, N is the [Ho^{3+}] concentration and N_C is the critical concentration (given in mol%). The results from this analysis are presented in Fig. 3. The desired parameters were obtained using a best-fit analysis and are given by $\eta_0 = 0.893$ and $N_C = 1.0$ mol%. The calculated dependence of the cross relaxation efficiency with the Ho^{3+} concentration for the $^5I_5$ level decay is unusual and suggests that this process was assisted by fast energy migration. In this case, the cross-relaxation process in the current samples is more efficient than it would be if it was assisted for example, by hopping migration.

3.2. Energy transfer upconversion from the $^5I_7$ level (ETU_1)

It is well known [10] that a non-radiative energy transfer process involving two interacting excited Ho^{3+} ions in the $^5I_7$ level promotes excitation to the $^5I_6$ level according to the process: Ho^{3+} ($^5I_7$) + Ho^{3+} ($^5I_7$) → Ho^{3+} ($^5I_6$) + Ho^{3+} ($^5I_8$) + pħω (p~3) (labelled the ETU_1 process). The ETU_1 rate constant (K_1) was obtained for the Ho^{3+}(x)-doped InF_3 glasses with x = 2, 4 and 10 mol.%. For this experiment, we used pulsed laser excitation at 1985 nm with the following excitation parameters: i) mean energy (E) of 9.3 mJ and focused beam area (A) equal to 0.0023 cm^2 for the 2 mol% sample, ii) E = 8.6 mJ and A = 0.0041 cm^2 for the 4 mol.% sample and iii) E = 6.5 mJ and A = 0.0041 cm^2 for the 10 mol.% sample. The smaller pump spot for the lower concentration sample provided an increase in the fluorescence signal and Fig. 4 shows the upconversion measurements.

Analysis of the upconversion luminescence transient for the $^5I_6$ level under $^5I_8$ → $^5I_7$ laser excitation at 1985 nm was performed using a best-fit analysis that employed the relationship [5].

$$I(t) = I_0\left\{ \exp\left(-\gamma_1\sqrt{t} - t/t_1\right) - \exp(-t/t_2) \right\}, \quad (4)$$

where γ_1, t_1 are the fitting parameters for the decay of the $^5I_6$ level and t_2 is the upconversion time. The ETU_1 rate i.e., W_{ETU1} (s^{-1}) was

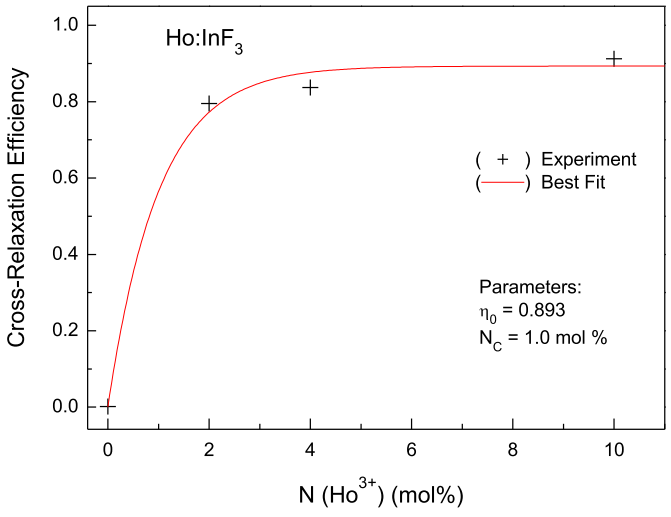

Fig. 3. Calculated cross-relaxation efficiency (η_{CR1}) as a function of the Ho^{3+} ion concentration. The solid red line represents the best-fit curve using the critical radius model described by Eq. (3). (For interpretation of the references to colour in this figure legend, the reader is referred to the web version of this article.)

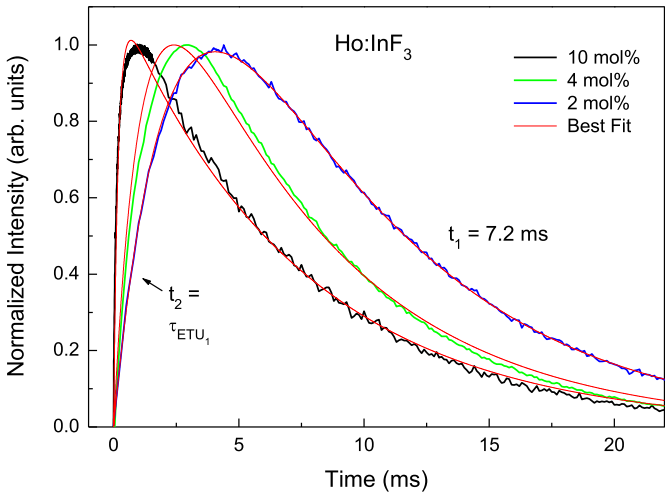

Fig. 4. Measured $^5I_6$ luminescence transient (at 1200 nm) due to the ETU_1 upconversion process induced by pulse laser excitation at 1985 nm with excitation conditions i) E = 9.3 mJ and excitation volume (V) equal to 0.00122 cm^3 for [Ho^{3+}] = 2 mol.%, ii) E = 8.6 mJ and V = 0.00217 cm^3 for [Ho^{3+}] = 4 mol.% and iii) E = 6.5 mJ and V = 0.00217 cm^3 for [Ho^{3+}] = 10 mol.%.

Table 2
Parameters obtained from the best-fit analysis for the upconversion luminescence from the $^5I_6$ level after laser excitation at 1985 nm.

[Ho^{3+}] (mol.%)	f(abs.) (λ = 1985 nm)	N^* (photons cm^{-3}) (exc. density)	t_1 (ms) ($\gamma_1 = 0$)	t_2 (ms)	R^2	W_{ETU1} (s^{-1})	K_1 (ETU_1) (s^{-1})
2	0.42	3.20×10^{19}	6.9	2.49	0.999	340	474
4	0.67	2.65×10^{19}	7.2	1.10	0.996	848	1723
10	0.94	2.90×10^{19}	7.3	0.184	0.997	5373	8913

f(abs.) is the absorption fraction (or absorptivity) of the $^5I_8 \rightarrow {}^5I_7$ absorption of Ho:InF_3 glass at the excitation wavelength of 1985 nm for an optical length of d = 5.3 mm (or sample thickness).

obtained using the relation $W_{ETU_1}(s^{-1}) = \frac{1}{t_2} - \frac{1}{\tau_d}$, where τ_d is equal to 16.3 ms, the intrinsic decay time of the $^5I_7$ level. Table 2 shows the parameters from the best-fit analysis (see coloured curves in Fig. 4) using the measured luminescence for the three Ho^{3+} concentrations.

Using the critical radius function given in our previous paper [5] we can obtain the ETU_1 rate constant K_1 for any Ho^{3+} concentration using

$$K_1 = \frac{W_{ETU_1}}{1 - \exp\left[-\frac{(N^* - N_0)}{N_{C_1}}\right]}, \quad (5)$$

where N^* is determined measured for each new sample with differing Ho^{3+} ion concentration, N_0 is equal to 2×10^{19} cm^{-3} and N_{C1} is equal to 9.51×10^{18} cm^{-3}. K_1 values were calculated using Eq. (2) and the W_{ETU1} rates and excitation densities (N^*) from Table 1. The calculated ETU_1 rates constants, K_1 are given in Table 2.

Fig. 5 shows the cross-relaxation rate constant K_1 as a function of the Ho^{3+} concentration. The solid black line shows the curve of best fit using a power law function given by $K_1 = a[Ho]^b$, where the best-fit parameters were $a = 100.2$ s^{-1} $(mol.\%)^{-b}$ and $b = 1.95$. The quadratic dependence of K_1 on the Ho^{3+} concentration is expected for an energy transfer process involving two ions in the same excited state (i.e., the $^5I_7$ level). If hopping migration is present, the energy transfer rate K_m is proportional to c_A c_D, where c_A and c_D are the acceptor and donor concentrations, respectively [11]. However, in the case of the ETU_1 process the acceptor and donor states are identical.

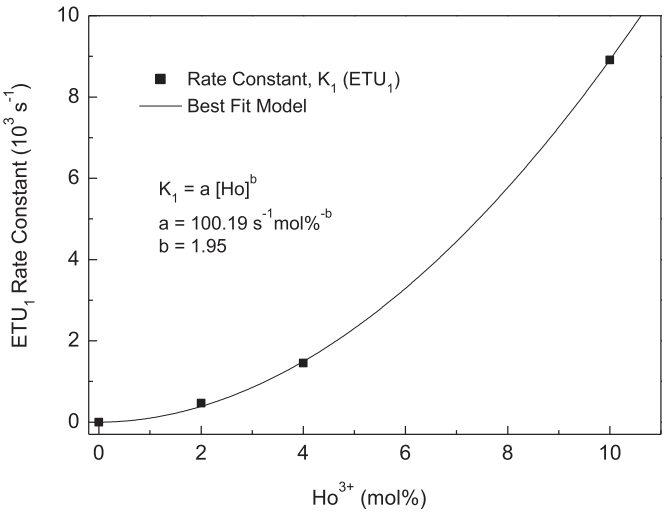

Fig. 5. Cross-relaxation rate K_1 as a function of the Ho^{3+} concentration. Solid black line shows the curve of best fit using a power law function.

3.3. Energy transfer upconversion from the $^5I_6$ excited level (ETU_2)

A non-radiative energy transfer involving two interacting excited Ho^{3+} ions in the $^5I_6$ level is also well known from previous studies [10]. The ETU process is described according to: Ho^{3+} ($^5I_6$) + Ho^{3+} ($^5I_6$) → Ho^{3+} ($^5F_5$) + Ho^{3+} ($^5I_8$) + pħω (p~3) (labelled the ETU_2 process). For this experiment, pulsed laser excitation at 1150 nm and a mean pulse energy of 9.3 mJ was focused to an area A = 0.0041 cm^2 for the all samples. Fig. 6 shows the measured upconversion luminescence curves measured after laser excitation at 1150 nm. The comparatively long time decay component (t_1, see Eq. (6)) is due to the ETU_2 process, which contributes to 48% of the total luminescence signal. The short decay time component (t_3, see Eq. (6)) is due to ESA absorption that populates the $^5S_2$ level, which

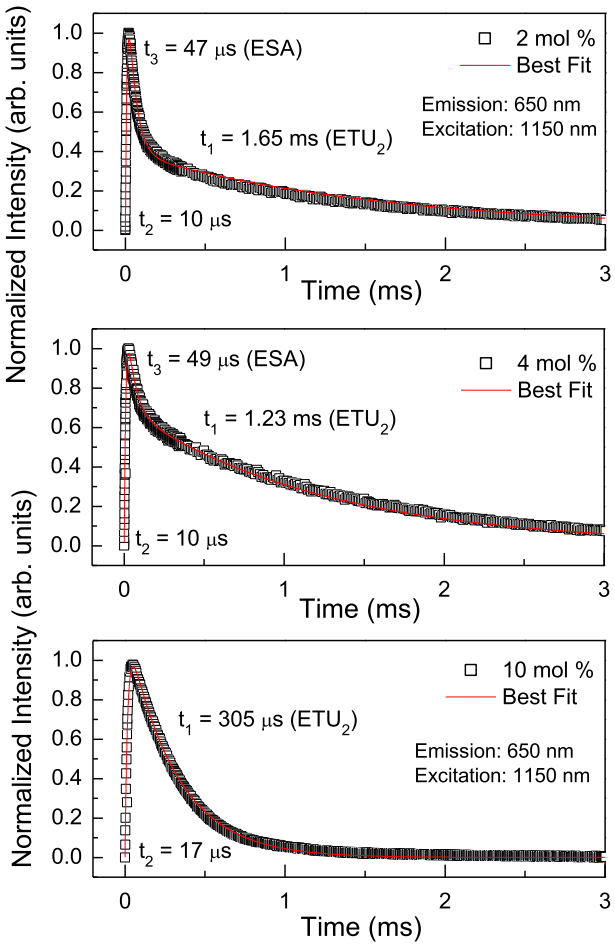

Fig. 6. Luminescence transient for emission from the $^5F_5$ level induced by ETU_2 process after laser excitation at 1150 nm (with a mean energy of 9.3 mJ and excitation volume V = 0.00217 cm^3) for InF_3 glass doped with (a) 2 mol.% Ho^{3+}, (b) 4 mol.% Ho^{3+}, and 10 mol.%. The fast decay component (t_3) relates to ESA that populates the $^5S_2$ level and subsequently the $^5F_5$ level.

in turn relaxes to the $^5F_5$ level and contributes to the luminescence decay at 650 nm. We calculate that the contribution from ESA is 76% for the Ho^{3+} (2 mol.%) doped sample and 52% for the Ho^{3+} (4 mol.%) doped sample. Excited state absorption at 1150 nm is negligible for the Ho^{3+} (10 mol.%) doped sample.

A best-fit analysis to the upconversion luminescence transient due to ETU_2 process after laser excitation at 1150 nm was performed using

$$I(t) = A\exp\left(-\gamma_1\sqrt{t} - t/t_1\right) - B\exp(-t/t_2) + C\exp(-t/t_3), \quad (6)$$

where γ_1, t_1 are the fitting parameters for the ETU_2 process, t_2 is due to the $^5F_5$ level decay and t_3 is due to the $^5S_2$ level decay after ESA. A, B and C are constants; B and C are used to determine the contributions from ETU_2 and ESA, respectively. Similarly, the rate of ETU_2 (in s^{-1}) can be obtained using the relation $W_{ETU_2}(s^{-1}) = \frac{1}{t_1} - \frac{1}{\tau_d}$, where τ_d is equal to 6.2 ms, the intrinsic decay of the $^5I_6$ level, as determined from our previous study [5]. Table 3 shows the parameters from the best-fit analysis for all concentrations studied.

The critical radius model that described ETU_2 as a function of the excitation density (N^*) from our previous study [5] of the Ho^{3+} (10 mol.%)-doped InF_3 sample was used to obtain the ETU_2 rate constant K_0 the 2 mol.% and 4 mol.% samples. The rate constant K_2 was obtained from

$$K_2 = \frac{W_{ETU_2}}{1 - \exp\left[-\frac{N^*}{N_{C_2}}\right]}, \quad (7)$$

where the critical concentration N_{C2} was determined to be 1.74×10^{19} cm^{-3}. Using the rate values for W_{ETU2} given in Table 3 for the 2 mol.% and 4 mol.% and the respective excitation densities (N^*) that were used, one can calculate the K_2 values, which are given in Table 3.

3.4. Excited state absorption from level $^5I_6$

It was observed, see Fig. 7, that green luminescence [from the $^5S_2$ ($^5F_4$) level] after pulsed excitation at 1150 nm (E = 11 mJ, 4 ns, 10 Hz) for all three Ho^{3+}-doped InF_3 samples. The rise time of the green luminescence tracked the pulse laser duration, which indicated that ESA was present by way of two photon absorption (TPA) $^5I_8 \rightarrow {}^5I_6$, $^5I_6 \rightarrow {}^5S_2$. The ESA transition ($^5I_6 \rightarrow {}^5S_2$) is not resonant with the 1150 nm excitation wavelength because the $^5I_6 \rightarrow {}^5S_2$ ESA process has a maximum at 962 nm (or centroid at approximately 965 nm) according to the energy level diagram for the Ho^{3+} ion. We postulate that laser excitation at 1150 nm excites the two-phonon sideband of ESA band similar to what has been observed for Ho^{3+}-doped ZBLAN glass [11].

The decay of the $^5S_2$ excited state shown in Fig. 7 behaves with a non-exponential characteristic with the parameter in Eq. (6) $\gamma \gg 0$ and using B = C = 0. The integrated lifetime τ_1(int), see Fig. 7 was much shorter for all samples than the radiative lifetime i.e., $\tau_R = 312$ μs calculated for this level. This fast decay arises from an effective

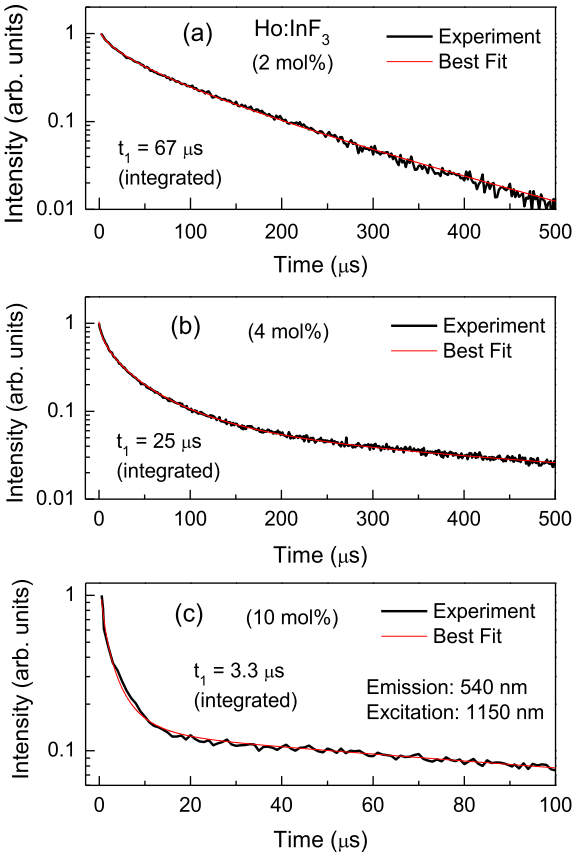

Fig. 7. Measured luminescence decay of the $^5S_2$ ($^5F_4$) level measured at 540 nm from TPA after pulsed laser excitation at 1150 nm (E = 11 mJ, 4 ns, 10 Hz) for [Ho^{3+}] = 2, 4 and 10 mol%. The fast decay component is due to the CR_2 process.

Table 4
Parameters from the best-fit analysis of the luminescence from $^5S_2$ level.

[Ho^{3+}] (mol.%)	γ($s^{-1/2}$)	t_1 (μs)	τ	R^2	W_{CR2} (s^{-1})
2	119	264	67	0.999	11720
4	241	200	25	0.999	36795
10	1169	60	3.3	0.993	2.998×10^5

cross-relaxation process (labelled CR_2) is described by Ho^{3+} ($^5S_2$) + Ho^{3+} ($^5I_8$) → Ho^{3+} ($^5I_4$) + Ho^{3+} ($^5I_7$). The cross-relaxation rate was calculated using the relation: $W_{CR_2} = \frac{1}{\tau_1(\text{int})} - \frac{1}{\tau_d}$, where $\tau_d = \tau_R$ [calculated in this work for the $^5S_2$ ($^5F_4$) level]. Table 4 shows the parameters from the best-fit analysis using the measured luminescence in Fig. 7. The W_{CR2} value for the 2 mol% Ho^{3+} sample can be compared with the value of 18000 s^{-1} for a 2% Ho^{3+}-doped InF_3 glass studied in Ref. [12] and 6580 s^{-1} for a 2.25% Ho^{3+}-doped InF_3 glass studied in Ref. [13].

The ESA absorption cross section (for $^5I_6 \rightarrow {}^5S_2$) was calculated using the McCumber method [14], which relates the emission and

Table 3
Parameters from the best-fit analysis for upconversion-induced luminescence transient from the $^5F_5$ level.

[Ho^{3+}] (mol%)	f(abs.)	N^* (cm^{-3})	t_1 (ms) ($\gamma_1 = 0$)	t_2 (μs)	t_3 (μs)	R^2	W_{ETU2} (s^{-1})	K_2 (ETU_2) (s^{-1})
2	0.39	0.98×10^{19}	1.65	10	47.4	0.997	445	1018
4	0.63	1.48×10^{19}	1.23	10	49.5	0.998	652	1138
10	0.91	2.35×10^{19}	0.305	17	–	0.998	3117	4212

f(abs.) is the absorption fraction (or absorptivity) of the $^5I_8 \rightarrow {}^5I_6$ absorption of Ho:InF_3 at λ = 1150 nm for an optical length of 5.3 mm (or sample thickness).

absorption cross-sections using the relation

$$\sigma_{abs}(\lambda) = \sigma_{emis}(\lambda)\ \frac{N_2}{N_1}\ \exp\left(-\frac{\hbar\omega}{k_B T}\right), \tag{8}$$

where $N_i = g_i\ \exp\left(-\frac{E_i}{k_B T}\right)$ and N_1 is the equilibrium population at T = 300 K for the initial level (i.e., $^5I_6$, at $E_1 = 8696\ cm^{-1}$) and N_2 is the final level (i.e., $^5S_2$, $^5F_4$ at $E_2 = 18994\ cm^{-1}$). The term g_i is the *i*-level degeneracy with values $g_1 = 13$ for the $^5I_6$ level and $g_2 = 14$ for the combined $^5S_2$, $^5F_4$ level. $\hbar\omega$ is the emission photon energy (in cm^{-1}), k_B is the Boltzmann constant and T = 300 K. Fig. 8 shows the measured emission cross-section spectrum obtained using the integration relation (described in our previous study [5]) and the calculated ESA absorption cross-section for the $^5I_6 \rightarrow {}^5S_2$, $^5F_4$ process. The maximum ESA cross section of $7.1 \times 10^{-21}\ cm^2$ occurs at 962 nm and is approximately sixteen times larger than σ_{GSA} ($= 4.3 \times 10^{-22}\ cm^2$) of the $^5I_8 \rightarrow {}^5I_5$ transition. Note that an ESA wavelength of 962 nm does not coincide with any GSA.

4. Rate equation analysis

Fig. 1 shows the energy level schematic presenting all the intrinsic and extrinsic processes involved when two pump wavelengths, at 889 and 962 nm are employed for laser emission at 3.93 μm. Note that the use of a two-wavelength pump scheme has been successfully employed for mid-infrared fibre lasers based on the Er^{3+} ion [15–17]. We label the pump wavelength at 889 nm (λ_{P1}) the primary pump and the excitation wavelength at 962 nm (λ_{P2}) the secondary pump.

In the model, we assume CW excitation at both pump wavelengths. The parameters n_1, n_2, n_3, n_4, n_5 and n_6 are used to represent the populations in the $^5I_8$, $^5I_7$, $^5I_6$, $^5I_5$, $^5F_5$ and $^5S_2$ energy levels of Ho^{3+}, respectively. These levels are considered the most important and relevant to the simulation of lasing at 3.93 μm. The $^5I_4$ level is strongly quenched by fast multiphonon decay and is therefore ignored. The rate equations for 889 nm pumping (assuming $n_1 + n_2 + n_3 + n_4 + n_5 + n_6 = 1$) are given by

$$\frac{dn_1}{dt} = -R_{P1}\ n_1 + \frac{\beta_{51}}{\tau_{R5}}n_5 + \frac{\beta_{41}}{\tau_{R4}}n_4 + \frac{\beta_{31}}{\tau_{R3}}n_3 + \frac{\beta_{21}}{\tau_{R2}}n_2 + \frac{\beta_{61}}{\tau_{R6}}n_6 + K_1 n_2^2 + K_2\ n_3^2 - W_{CR1}\ n_1\ n_4 - W_{CR2}\ n_1\ n_6 \tag{9}$$

$$\frac{dn_2}{dt} = \frac{\beta_{52}}{\tau_{R5}}n_5 + \frac{\beta_{42}}{\tau_{R4}}n_4 + \frac{\beta_{32}}{\tau_{R3}}n_3 + \frac{\beta_{62}}{\tau_{R6}}n_6 - \frac{1}{\tau_{R2}}n_2 - 2\ K_1 n_2^2 + 2\ W_{CR1}\ n_1\ n_4 + W_{CR2}\ n_1\ n_6 + W_{NR}(32)\ n_3 \tag{10}$$

$$\frac{dn_3}{dt} = -\frac{n_3}{\tau_{R3}} - W_{NR}(32)\ n_3 + W_{NR}(43)\ n_4 + \frac{\beta_{43}}{\tau_{R4}}n_4 + \frac{\beta_{53}}{\tau_{R5}}\ n_5 + \frac{\beta_{63}}{\tau_{R6}}n_6 + K_1\ n_2^2 - 2\ K_2\ n_3^2 - R_{P2}\ n_3 \tag{11}$$

$$\frac{dn_4}{dt} = R_{P1}\ n_1 - \frac{n_4}{\tau_{R4}} + W_{NR}(54)\ n_5 - W_{NR}(43)\ n_4 - W_{CR1}\ n_1\ n_4 + W_{CR2}\ n_1\ n_6 \tag{12}$$

$$\frac{dn_5}{dt} = -\frac{n_5}{\tau_{R5}} - W_{NR}(54)\ n_5 + K_2\ n_3^2 \tag{13}$$

$$\frac{dn_6}{dt} = R_{P2}\ n_3 - W_{CR2}\ n_1\ n_6 - \frac{n_6}{\tau_{R6}} \tag{14}$$

where $R_{Pi} = \sigma_{14}\ \frac{I_{Pi}}{(h\nu)_{Pi}}$ is the pump rate (in s^{-1}), I_{P1} is the pump light (in W cm^{-2}), and $h\nu$ is the pump photon energy. β_{ij} represents the luminescence branching ratio and τ_{Ri} is the radiative lifetime of the excited states of Ho^{3+} (labelled as *i* = *2*, *3*, *4*, *5* and *6*). The absorption and emission cross-sections are $\sigma_{14} = 4.3 \times 10^{-22}\ cm^2$ (GSA at 889 nm), $\sigma_{36} = 7.1 \times 10^{-21}\ cm^2$ (ESA at 962 nm) and $\sigma_{43} = 3.7 \times 10^{-21}\ cm^2$ (at 3925 nm). All other parameters are given in Table 5. Note that the value for τ_d for the $^5S_2$ level in Table 5 is longer than the value of 105 μs for the same energy level given in Ref. [13].

Numerical solution of the rate equations was carried out to understand the potential for efficient laser emission at 3.93 μm under two wavelength CW pumping. The calculated evolution of the population inversion [($n_4 - n_3$), in mol.%] was obtained by numerical simulation of the rate equations for [Ho^{3+}] = 2, 4 and 10 mol.%. Using the primary pumping rate (R_{P1}) of 2000 s^{-1} and several secondary-pumping rates (R_{P2}, is the secondary pump rate) from 2×10^3 to $6 \times 10^4\ s^{-1}$ the population inversion was calculated as shown in Figs. 9–11. The calculations show that a positive steady sate population inversion is obtained 2 ms after initiation of the primary pump for values of the secondary pumping rate $R_{P2} > 1 \times 10^4\ s^{-1}$. The secondary pumping at 962 nm first depopulates the lower ($^5I_6$) laser level and for higher values for R_{P2}, it contributes to excitation of the upper ($^5I_5$) laser level population.

Fig. 12 shows the calculated population inversion (n_4-n_3) obtained at equilibrium (after 3 ms) as a function of R_{P2} for constant $R_{P1} = 2000\ s^{-1}$ and [Ho^{3+}] = 2, 4 and 10 mol.%. The results suggest that the [Ho^{3+}] = 10 mol.% is the best concentration for achieving CW laser operation at 3.93 μm with double wavelength pumping because the population inversion fraction of 15% (when $R_{P2} = 6 \times 10^4\ s^{-1}$) is certainly sufficient to overcome the laser cavity losses relevant to a practical system. The pump intensity (I_{Pi}) can be calculated using $I_{Pi} = \frac{h\nu\ R_{Pi}}{\sigma_{abs}}$, where $h\nu$ is the photon excitation energy (in joules) and σ_{abs} is the absorption cross-section (cm^2) (at wavelength excitation λ_{Pi}). Table 6 shows the values used for this

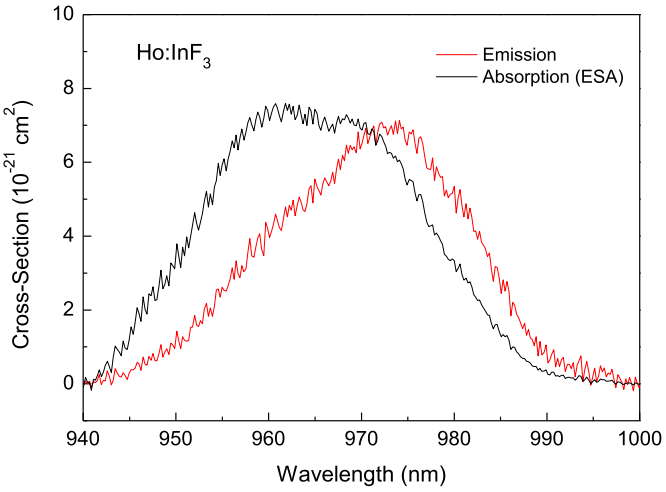

Fig. 8. Measured emission cross-section for the ($^5S_2$, $^5F_4$) → $^5I_6$ transition after pulsed laser excitation at 1150 nm (E_p = 11 mJ). The corresponding ESA cross-section (black curve) was obtained using the McCumber method given by Eq. (8).

Table 5
Parameters used in the rate equation modelling.

Luminescence branching ratio and radiative and intrinsic (total) lifetimes of Ho^{3+}			
Transition (level#)	β[a]	τ_R[b]	$\tau_d = \tau$(intrinsic)[c] (W_{NR} (s^{-1}))
$^5S_2$ (6) →		312 μs	τ_d = 312 μs (W_{NR} (65) = 0)
$^5I_6$ (3)	0.10		
$^5I_7$ (2)	0.40		
$^5I_8$ (1)	0.50		
$^5F_5$ (5) →		321 μs	$\tau_d = \tau$ = 16.3 μs (γ = 0) (W_{NR} (54) = 58234 s^{-1})
$^5I_5$ (4)	0.004		
$^5I_6$ (3)	0.046		
$^5I_7$ (2)	0.192		
$^5I_8$ (1)	0.758		
$^5I_5$ (4) →		6.8 ms	τ_d = 135 μs (W_{NR} (43) = 7260 s^{-1})
$^5I_6$ (3)	0.013		
$^5I_7$ (2)	0.430		
$^5I_8$ (1)	0.557		
$^5I_6$ (3) →		6.2 ms	$\tau_d = \tau$ = 6.2 ms (γ = 0) (W_{NR} (32) = 0)
$^5I_7$ (2)	0.058		
$^5I_8$ (1)	0.942		
$^5I_7$ (2) → $^5I_8$ (1)	1	16.2 ms	τ_d = 16.2 ms (W_{NR} (21) = 0)

Energy transfer rate parameters (s^{-1}) (expt.)[d]				
$Ho:InF_3$(mol.%)	ETU_1 K_1 (s^{-1})	ETU_2 K_2 (s^{-1})	CR_1 W_{CR1} (s^{-1})	CR_2 W_{CR2} (s^{-1})
2%	474	1018	25926	11720
4%	1723	1138	34259	36795
10%	8913	4212	69516	2.998×10^5

[a] Branching ratios calculated in this work.
[b] Radiative lifetimes calculated using Judd-Ofelt theory in this work.
[c] Experimental lifetime (intrinsic) obtained from the best fit to the luminescence done in this work.
[d] Experimental transfer rates obtained in this work.

numerical simulation.

5. Discussion

This study has quantified all the important energy transfer processes relevant to the operation of the $^5I_5 \rightarrow {}^5I_6$ transition at 3930 nm. Accessing transitions between high lying energy levels typically involves a greater number of energy transfer processes because a greater number of energy levels are potentially populated. The $^5I_5 \rightarrow {}^5I_6$ transition is no exception and the present study has established that at least two energy transfer upconversion and two cross relaxation processes contribute to the emission from the $^5I_5 \rightarrow {}^5I_6$ transition. This investigation also comprises the most detailed spectroscopic study of a rare earth doped indium fluoride glass and allows future more detailed numerical simulation of laser systems based on this optical material.

The numerical simulations presented in this study suggest that double clad indium fluoride fibre that contains high concentrations of Ho^{3+} ions can be useful for high power CW emission at 3.93 μm. In our previous study [5], we showed that CR has the effect of significantly shortening the lifetime of the $^5I_5$ level which prevents, from a basic numerical simulation perspective, CW emission at high Ho^{3+} concentrations. We have shown in this study, however, that

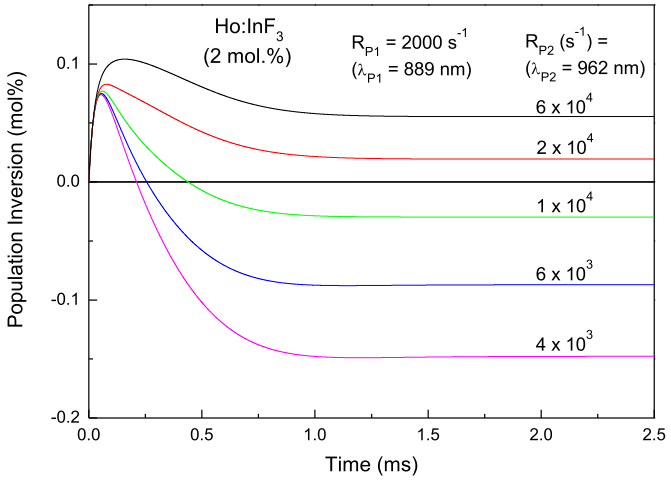

Fig. 9. Calculated population inversion (in mol.%) for the laser transition $^5I_5 \rightarrow {}^5I_6$ (at 3925 nm) as a function of the pumping intensities for $[Ho^{3+}]$ = 2 mol.% doped fluorindate glass under CW pumping at 889 nm (λ_{P1}) and CW pumping at 962 nm (λ_{P2}) (ESA) at 300 K. R_{P1} = 100 s^{-1} corresponds to a pump intensity (I_{P1}) equal to 51 KW cm^{-2} and R_{P2} = 100 s^{-1} corresponds to 3.25 KW cm^{-2} (I_{P2}).

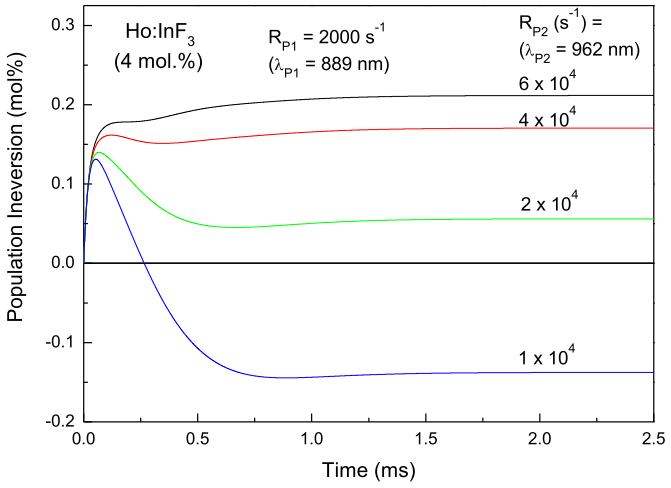

Fig. 10. Calculated population inversion (in mol.%) for the laser transition $^5I_5 \rightarrow {}^5I_6$ (at 3925 nm) as a function of the pumping intensities for $[Ho^{3+}]$ = 4 mol.% doped fluoroindate glass under CW pumping at 889 nm (λ_{P1}) and CW pumping at 962 nm (λ_{P2}) (ESA) at 300 K.

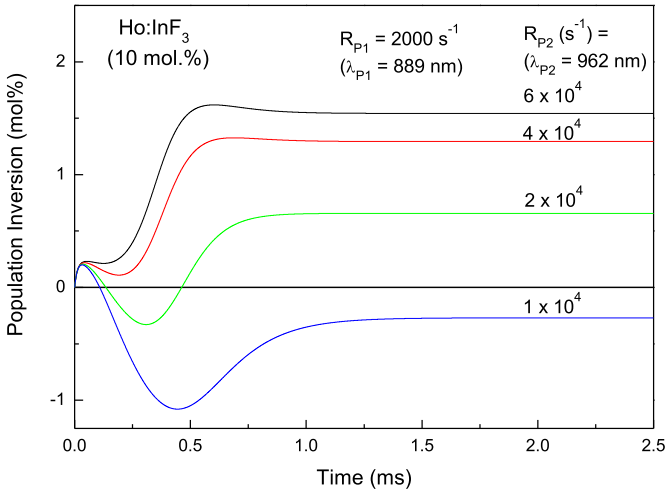

Fig. 11. Calculated population inversion (in mol.%) for the laser transition $^5I_5 \rightarrow {}^5I_6$ (at 3925 nm) as a function of the pumping intensities for $[Ho^{3+}]$ = 10 mol.% doped fluorindate glass under CW pumping at 889 nm (λ_{P1}) and CW pumping at 962 nm (λ_{P2}) (ESA) at 300 K.

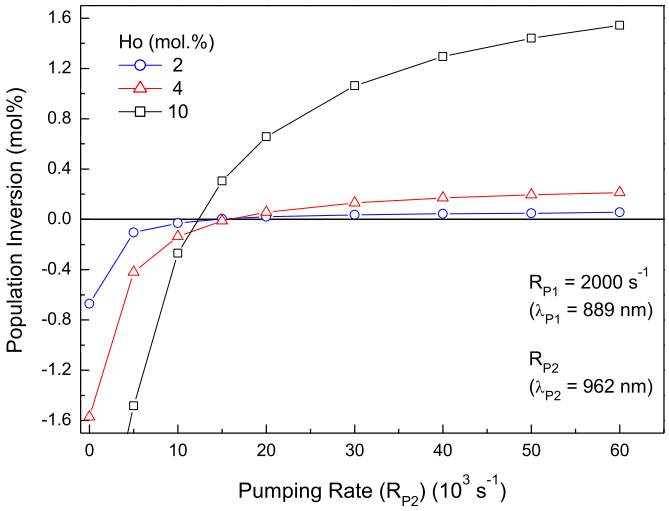

Fig. 12. Calculated population inversion (in mol.%) as a function of the pumping rate R_{P2} at $\lambda_{P2} = 962$ nm for constant pumping (R_{P1}) at $\lambda_{P1} = 889$ nm for [Ho^{3+}] = 2, 4 and 10 mol.%.

Table 6
Wavelengths, absorption cross-sections for GSA and ESA processes, pumping rate and pumping intensity used in the numerical simulations for the 3.93 μm laser emission in Ho^{3+}-doped InF_3 glass.

$\lambda_{P1} = 889$ nm	$\sigma_{abs} = 4.4 \times 10^{-22}$ cm^{-2}
$\lambda_{P2} = 962$ nm	$\sigma_{ESA} = 7.1 \times 10^{-21}$ cm^{-2}
$R_{P1} = 2 \times 10^3$ s^{-1}	$I_{P1} = 1020$ KW cm^{-2}
R_{P2} (s^{-1})	I_{P2} (KW cm^{-2})
2×10^3	65
4×10^3	130
6×10^3	195
1×10^4	324
2×10^4	648
6×10^4	1945

with an additional pump characterised by a centre wavelength close to the ESA peak at 962 nm, that efficient CW laser emission is possible even for Ho^{3+} concentrations as high as 10 mol.%. This is a significant step forward because high power diode lasers at both 976 nm and 899 nm are available. The present study indicates that CW emission at 3930 nm beyond the one-watt level is a strong possibility, however, given the high pump rates used in the calculations, core pumping may be necessary. A complete fibre and experimental layout must wait, however, until a more accurate and complete numerical modelling study of dual wavelength pumping of Ho^{3+}-doped InF_3 glass optical fibre has been carried out.

6. Conclusions

We have reported a detailed time-resolved spectroscopic study of Ho^{3+}-doped indium fluoride glass relevant to the emission from the $^5I_5 \rightarrow {}^5I_6$ transition at 3930 nm. The rate parameters for all the relevant energy transfer processes have been determined. These rates are useful for modelling laser systems based on either fibre or bulk geometries. We have shown that under dual wavelength pumping, Ho^{3+}-doped InF_3 glass fibres have the potential to enable CW laser emission at 3930 nm for concentrations ranging from 2 mol.% to 10 mol.%, despite the presence of strong cross relaxation that can effectively quench the upper laser level. We have established that a Ho^{3+} concentration of 10 mol.% provides the highest fractional population inversion (of 15%) for an ESA pumping rate $R_{P2} = 6 \times 10^4$ s^{-1}. Given the low background loss at 3.9 μm (of approximately 20 dB km^{-1}) combined with secondary pumping in the 970 nm region, we expect that a fibre doped with 10 mol.% Ho^{3+} will provide a viable route to moderate power generation at 3.9 μm.

Acknowledgments

The authors thank the financial support from São Paulo State Research Foundation (FAPESP, Grants N^0 1995/4166-0 and 2000/10986-0), the Brazilian Research Foundation (CNPq), the Australian Research Council (DP140101336) and the Natural Sciences and Engineering Research Council of Canada.

References

[1] J. Schneider, Electron. Lett. 31 (1995) 1250.
[2] J. Schneider, C. Carbonnier, U.B. Unrau, Appl. Opt. 36 (1997) 8595.
[3] A. Berrou, C. Kieleck, M. Eichhorn, Opt. Lett. 40 (2015) 1699.
[4] See http://leverrefluore.com/.
[5] L. Gomes, V. Fortin, M. Bernier, R. Vallée, S. Poulain, M. Poulain, S.D. Jackson, Opt. Mat. 60 (2016) 618.
[6] M.A. Poulain, M.J. Poulain, Mat. Sci. Forum 32–33 (1988) 137.
[7] G. Mazé, M. Poulain, J. Y. Carrée, A. Soufiane, Y. Messaddeq, "Indium Fluoride glasses" US Patent N° 5480845.
[8] M. Poulain, A. Soufiane, Y. Messaddeq, M.A. Aegerte, Braz. J. Phys. 22 (1992) 205.
[9] A. Soufiane, F. Gan, H. L'Helgoualc'h, M. Poulain, J. Non-Crystalline Solids 184 (1995) 103.
[10] A.F.H. Librantz, S.D. Jackson, L. Gomes, S.J.L. Ribeiro, Y. Messaddeq, J. Appl. Phys. 103 (2008) 023105.
[11] R.C. Powell, Physics of Solid-state Laser Materials, Section 5.2-Nonradiative Energy Transfer : Multistep Process, AIP Press, New York, 1998, p. 203.
[12] N. Rakov, G.S. Maclel, C.B. De Araújo, Y. Messaddeq, Appl. Phys. 91 (2002) 1272.
[13] F. Lahoz, I.R. Martín, A. Briones, J. Appl. Phys. 95 (2004) 2957.
[14] D.E. McCumber, Phys. Rev. 136 (4A) (1968) 954.
[15] O. Henderson-Sapir, J. Munch, D.J. Ottaway, Opt. Lett. 39 (2014) 493–496.
[16] V. Fortin, F. Maes, M. Bernier, S.T. Bah, M. D'Auteuil, R. Vallée, Opt. Lett. 41 (2016) 559–562.
[17] O. Henderson-Sapir, S.D. Jackson, D.J. Ottaway, Opt. Lett. 41 (2016) 1676–1679.